Proceedings of the Design Society, Volume 5: ICED25
https://doi.org/10.1017/pds.2025.10297

Scaling generative design for production through the use of standard parts

Jonathan Raines ,✉, **David Barton** and **Ben Hicks**

University of Bristol, UK,

✉ jonathan.raines@bristol.ac.uk

ABSTRACT: Generative Design (GD) tools can produce high-performing components with complex geometries that are challenging to conceive via traditional methods. While potentially disruptive, GD tools have yet to achieve widespread use in industry. One reason is that current GD tools are limited to manufacturing methods capable of producing intricate geometries that GD often creates such as 3D printing. To overcome this barrier, this paper quantifies the benefit of altering generatively designed parts to use standardized elements like wire stock and sheet metal via processes such as CNC bending and water jet cutting. Using a parametric cost model, we show that parts incorporating standard components can halve the unit price for production volumes of only 4 parts. Finite Element Analysis (FEA) reveals that replacing up to 60% of part volume has minimal impact on performance. Our findings highlight a gap and opportunity in existing GD research.

KEYWORDS: Design methods, Computer Aided Design (CAD), Design for X (DfX)

1. Introduction

Generative Design (GD) represents a promising frontier in engineering, employing sophisticated algorithms to derive near optimal solutions for complex physical design challenges. However, current GD tools primarily output monolithic, free-form components that, while geometrically elegant, may present significant manufacturing challenges.

Leading software solutions, such as Autodesk Fusion (Autodesk, 2024), incorporate manufacturing constraints for additive manufacturing, casting, and machining. Yet this relatively narrow focus can significantly inflate both production costs and complexity. More economical manufacturing processes, such as sheet metal bending, remain largely unexplored in the GD space, as does the strategic incorporation of standard components.

The industrial engineering community has long recognised the cost-saving benefits of standardised, off-the-shelf parts. Contemporary consumer products typically comprise 30% standard components, while more complex machines, such as bicycles, may incorporate upwards of 70% standard parts (Hicks et al., 2002). Manufacturing with standard parts has consistently demonstrated advantages in cost reduction, accelerated production timelines, and streamlined testing processes. This paper examines a simple bracket as a case study to investigate the research question:

> *How does the inclusion of standard parts affect the cost and performance of a generatively designed part.?*

Section 2 presents a review of current GD tools and their manufacturing considerations. Section 3 details the methodology used, including the bracket selection criteria, manual redesign process, and analytical approaches for deflection and mass measurements. Finally, section 4 and section 5 present our findings and discuss their broader implications for the future.

Our research challenges the current paradigm in generative design and proposes a more balanced approach that considers both geometric optimisation and manufacturing practicality.

2. Related work

This section provides a brief background on generative design and topology optimisation to contextualise the limitations examined in this work. It reviews previous research examining the benefits of using standard parts and covers existing work on integrating components into topology optimisation - the primary motivation for this study.

Generative design is the process of algorithmically generating and evaluating multiple solutions to a design problem. Within mechanical design, Topology Optimization (TO) is a well-studied method of generating designs. Currently, an active research community is working to achieve real-time implementation of these methods. Approaches include directly predicting results from input conditions using machine learning (Yu et al., 2019; Nie et al., 2020; Hoang et al., 2022), training surrogate models to replace Finite Element Analysis (FEA) (Sasaki and Igarashi, 2019; Seo and Kapania, 2022), and using machine learning to accelerate traditional FEA (Huang et al., 2023). While computational cost remains a significant barrier to adoption, the manufacturability and economic viability of generated parts present equally important challenges.

Manufacturability itself constitutes an active field of research. Indeed, Autodesk Fusion (Autodesk, 2024), the commercial generative system employed in this study, already incorporates constraints for 3D printing, machining and casting. While the exact implementation in closed-source software remains proprietary, the literature demonstrates that constraints ensuring a draft angle for casting have been implemented by modifying the optimisation used in Solid Isotropic Material with Penalization (SIMP) to consider a 2D projection of the part (Yoon and Ha, 2020). Researchers have modified density-based methods (such as SIMP) to respect minimum feature size and overhang constraints of 3D printing (Bar-roqueiro et al., 2019; Fernández et al., 2020; Weiss et al., 2018). More recently, researchers taken used a similar approach to impose constraints for 2.5 and 5 axis machining, using projections to penalize areas inaccesible to the tool during optimisation Lee et al. (2022). Greminger (2020) adopted a data-driven approach, training a Generative Adversarial Network (GAN) on examples of machinable parts. The TO was then performed in the latent space of the GAN, effectively constraining it to manufacturable solutions. These techniques exclusively apply to manufacturing processes that take a bulk material as input: blanks for machining, powder for 3D printing, and molten metal for casting. Making use of stock materials such as bar or sheet, as per this case study, requires a rephrasing of the problem. GD systems will need to handle a wide range of processes to be useful across industry.

The use of standard parts to reduce costs has been established wisdom since at least 1984 (Pahl and Beitz, 1984). Standard parts from third-party suppliers typically offer higher quality and lower costs compared to custom components. These suppliers can leverage greater economies of scale while investing in refined production processes (Ulrich and Eppinger, 2000). Additional benefits include enhanced supply chain resilience (Hicks and Culley, 2002).

Research on component integration broadly falls into two categories: those applying post-processing steps to existing GD techniques (similar to a substitution operation) and those directly generating designs using components.

Watson et al. (2023) developed a workflow for replacing parts of a generative design with standard components. Similar to the bracket examined in this paper, they observed that generatively designed parts constrained with a low volume fraction (<0.2) tend to exhibit strut-like features. Their method involves skeletonising the part, generating a Computer-Aided Design (CAD) model, and optimising the model parameters. Recent research has applied Machine Vision techniques to classify areas of 2D parts as struts (Rochefort-Beaudoin et al., 2024).

Conversely, Moveable Morphable Components (MMC) (Guo et al., 2014; Zhang et al., 2016)—an extension of SIMP (Bendsøe and Kikuchi, 1988)—exemplifies the direct component approach. Rather than implicitly representing designs as images, it employs explicit collections of parametric components. These components generate image-like representations using Topology Description Functions (TDFs). The iterative pixel-wise improvements to part performance from SIMP are then backpropagated to the

components' design parameters. While MMC was initially developed to provide better control over generated features (e.g., minimum features size (Weiss et al., 2018)) and improve relationships between TO output and CAD representations, researchers have recently begun exploring how components can be defined to reflect manufacturing processes (Li et al., 2024).

3. Methodology

This section details the approach of this case study. The approach consists of 6 stages. The first three stages produce the parts that are analysed in the subsequent three stages. The method is illustrated graphically in figure 1.

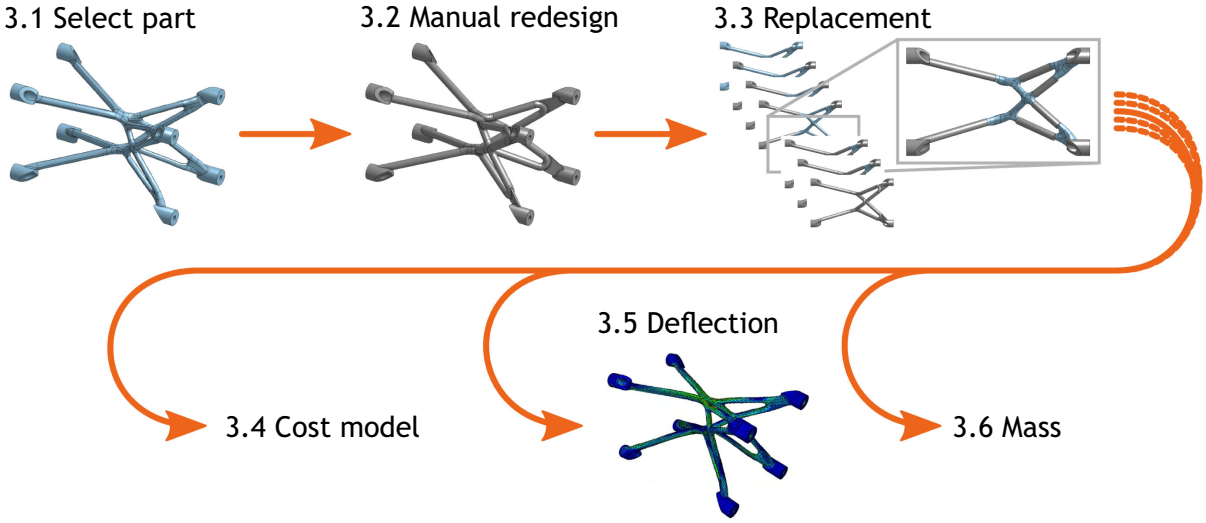

Figure 1. Method Diagram

3.1. Select part

The part used in this case study is a bracket for mounting a load, such as a television, a fixed distance off a wall. It was generated using Autodesk Fusion (Autodesk, 2024). The bosses for the bolts in each corner were defined as "keep geometry". The material was set to Aluminium. No manufacturing constraint was imposed.

This part was chosen to emphasize a limitation of current GD tools. It is large, making it expensive to 3D print (see section 4.1). It is also rarefied (its volume is a small proportion of its bounding box) meaning if machined, most of the billet of material would become waste swarf. Finally, its geometry makes casting extremely difficult.

3.2. Manual redesign

The objective of redesigning the generative part was to reduce its cost by mimicking the geometry using commercially available stock. For the purposes of this case study, we deemed bar or wire to be the most appropriate stock material. CNC wire bending was selected as the main manufacturing process. Some machining, brazing, and water jet cutting were also required. The replacement part was designed in Onshape (PTC Inc, 2024, version 1.190) using the generative part as a reference. There are multiple ways the original part could be approximated, a sheet metal option not analysed in this work is shown in figure 2. A future automated system, which this paper advocates for, should aim to compare a Pareto front of optimal options. For this study, wire forming was chosen as the bar stock closely approximated the generative part's geometry and wire bending is a commonly used manufacturing process for space-frame like structures.

3.3. Replacement

Sections of the generatively designed part were replaced with parts made from stock material over seven stages. The stages are shown in figure 3 and details of each stage are shown in table 1.

The logic for the order in which sections were replaced is as follows. Reverse engineering the pricing model of OnSite (Materialise, 2024), a web-based instant quotation tool, revealed that the volume of

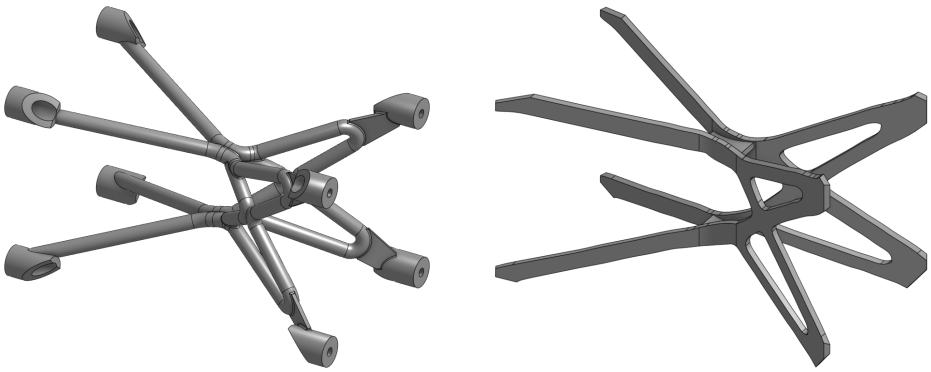

Figure 2. Left: the manually redesigned part analysed in this paper. Right: An alternative approximation of the generatively designed bracket using water jet cutting and bending only. It highlights the significant freedom in the redesign afforded by a wide range of manufacturing methods

Table 1. Replacement steps

Process	Part	Volume replaced (mm^3)	Volume Fraction	Step
Machining	Bosses	13739	37%	1
Wire cutting	Ground-side upper struts	4368	12%	2
Wire cutting	Ground-side lower struts	4122	11%	3
Wire cutting	Load-side struts	4730	12%	4
Wire bending	Centre joints	4072	11%	5
Wire bending	Inner section	2012	5%	6
Water jet cutting	Load-side bends	4155	11%	7

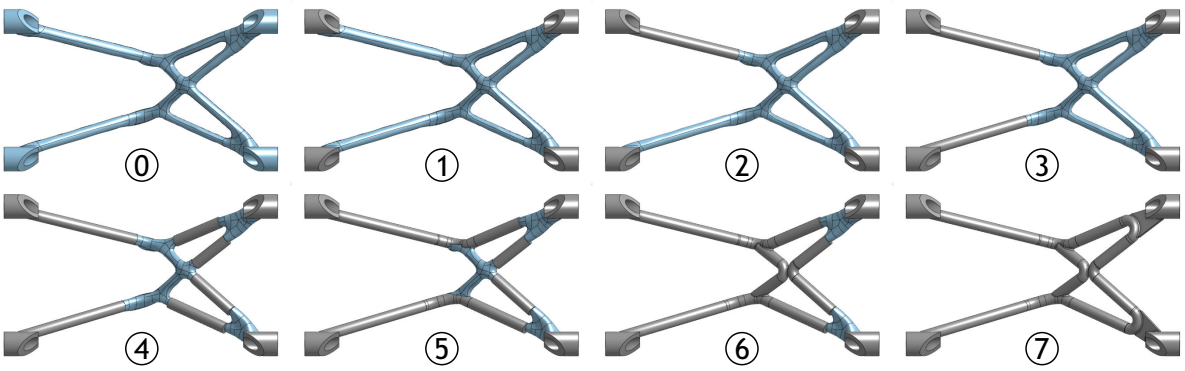

Figure 3. The original part (step 0) and the 7 replacement steps. The original generative part is shown in light blue, replacement parts in grey

printed parts is the primary driver of cost. The bounding box of the parts is a secondary driver. Therefore, the objective of reducing the cost reduction is best served by reducing the total volume of printed parts in an assembly. However, replacing parts necessitates the introduction of alternative processes, and these often have a setup cost. Hence, the sections of the generative part were grouped by process, then processes were introduced in order of the sum of the volumes they could replace. The result is that at each step, the largest volume of generated part is replaced for the fewest introduced new processes.

3.4. Cost model

The costs for the 3D printed part were obtained from the online 3D printing service Materialise (2024) using their instant online quotation. Their service takes into account part volume, bounding box, and surface finish. The parts were uploaded as 3MF files (a mesh format) (3MF Consortium, 2021). The

quotations were generated based on using metal 3D printing technology, standard performance aluminium (AlSil0Mg) and a corundum-blasted finish. Prices were taken including VAT and the online ordering discount (10%). Materialise state there is no bulk discount for this service, so the cost of parts was assumed to scale proportionally to the number of parts.
A parametric cost model was created to estimate the costs of the other processes, such as wire bending, at different production volumes. To account for uncertainty, the model uses a range and step size for each parameter, and computes all possible combinations of parameters. The minimum, maximum, and mean costs for each quantity are reported. Machining was costed according to equation (1)

$$C_s + \left\lceil \frac{Q}{\lambda_J} \right\rceil C_J + Q(C_m^l L + C_h t) \tag{1}$$

Where C_s, C_J, C_m, and C_h are the one-off setup cost, the price of any jigs required, the material cost per length, and the hourly cost of running the machine (including labour) respectively. λ_J is the lifetime of the jig. Q is the quantity of parts being made. \x\ represents rounding up, i.e. 'ceil(x)'. L and t are properties of the assembly being fabricated. They are the length of bar stock needed and the time required per part respectively.
Wire bending is costed using equation (2)

$$C_s + Q(C_m^l L + C_b N_b + C_c N_c) \tag{2}$$

Where C_s, C_m^l, C_b, and C_c are the one-off setup cost, the material cost per length, the cost per bend, and the cost per cut respectively. L, N_b, and N_c are parameters of an assembly. They are the length of wire used, the number of bends, and number of cuts. Q is the quantity of units in the production run. Brazing joints are costed using equation (3)

$$C_S + \left\lceil \frac{Q}{\lambda_J} \right\rceil C_J + C_j N_j Q \tag{3}$$

Where C_s, C_J and C_j are the setup cost, cost per jig, and cost per joint. X_J is the lifetime of the jig in terms of the number of assemblies it can make. N_j is the number of joints in an assembly. Finally, water jet cut parts are costed according to equation (4)

$$C_s + Q\left(\frac{L_p C_h}{F} + C_m^a A\right) \tag{4}$$

Where C_s is the setup cost. C_h is the hourly rate of running the machine as estimated using a web-based water jet cut calculator (Hypertherm Inc., USA, 2024) based on the electricity, water, cutting media use; as well as replacement part costs amortised per hour. C_m^a is the cost of material per unit area, the value of which was based on purchasing a 2 m by 1 m sheet of 3 mm thick aluminium. The assembly parameters are the perimeter length, L_p, and the area, A of material. A summary of all the variables and the value ranges used is shown in table 2.

3.5. Deflection and stress

Part deflection was estimated using a linear static FEA using Abaqus CAE (Dassault Systèmes, 2024, 2024 version). The analysis was run assuming the same boundary conditions as used to generate the original part. Namely, the ground-side boltholes were fixed in translation and rotation using an *encastre* constraint, and the load-side boltholes had a 200 N traction load applied vertically downwards. Additionally, the load-side boltholes were constrained to have no relative motion or rotation to simulate being fixed to a rigid body (the load). Assemblies were imported to Abaqus from Onshape using the.sldprt format as one part. The brazed joints between parts in the assemblies were approximated with a 1 mm radius fillet. These brazed joints were assigned the same material properties as the bracket material (as if it were one part). The analysis assumed the parts were aluminium, using a Poisson's ratio of 0.33, a Young's modulus of 68.9 GPa, a tensile yield strength of 27.6 MPa of and an ultimate tensile strength of 68.9 MPa. The parts were meshed using tetrahedral quadratic elements. The maximum deflection magnitude across the part was used as the performance metric. The same analysis was used to estimate the von Mises stress across the part. Similarly to the deflection, the maximum stress magnitude across the part was used as the performance metric.

Table 2. Cost model parameters.

Process	Parameter	Value / Range	Unit
Machining	Setup Cost (C_s)	50 to 150	GBP
	Jig Cost (C_J)	0 to 100	GBP
	Jig Life (λ_T)	1000	GBP
	Material cost per length (17.5 mm bar) (C_m^l)	6 to 10*	GBP/m
	Cost per hour (C_h)	15 to 36	GBP/m
Wire bending	Setup cost (C_s)	50 to 500	GBP
	Tool cost (C_T)	0 to 500	GBP
	Tool life (λ_T)	1000	bends
	Material cost per length (8 mm bar) (C_m^l)	1 to 5*	GBP/m
	Cost per bend (C_b)	0.1 to 2	GBP/bend
	Cost per cut (C_c)	0.1 to 1	GBP/cut
Brazing	Setup cost (C_s)	0 to 50	GBP
	Jig life (λ_J)	1000	parts
	Jig cost (λ_J)	0 to 100	GBP
	Cost per joint (C_j)	1 to 10	GBP
Water jet cutting	Setup cost (C_s)	0 to 50	GBP
	Hourly cost (C_h)	10 to 15	GBP/h
	Feed rate (F)	1300 to 26000	mm min^{-1}
	Material cost per area (C_m^a)	0.0364†	GBP/mm^2

*:*data sourced from (Aluminium Online, 2024).*
†:*data sourced from (Metals Warehouse, 2024)*

3.6. Mass

The mass of the parts was estimated simply by multiplying the volume of the parts by the density of aluminium (2.7×10^{-6} kg mm^{-2}). The volume of the parts was taken from the CAD system (Onshape).

4. Results

This section presents the analysis of both cost and performance metrics across the different design iterations. The cost analysis examines the unit costs and economies of scale for different production volumes, while the performance analysis compares structural characteristics including deflection, mass, and stress distribution. The results demonstrate the trade-offs between manufacturing cost and mechanical performance as the design transitions from fully 3D printed to conventional manufacturing methods.

4.1. Cost

The unit cost of the generated bracket made using metal 3D printing remains constant due to the lack of any economy of scale. For the step 7 part, manufactured entirely without 3D printing, the unit cost curve in figure 4 exhibits the expected asymptotic decrease as set-up costs are amortised and the price trends towards the sum of the per-unit costs for each component.

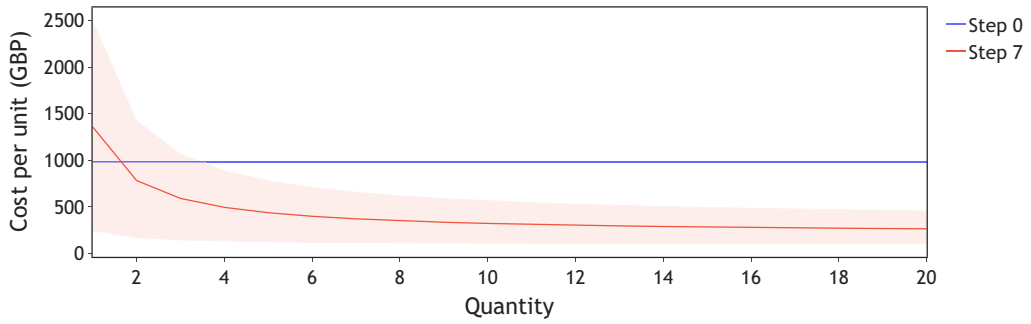

Figure 4. [Cost per unit between 1 and 20 units for each of the different steps. Step 0 is a flat line as the metal 3D printing process does not have any economies of scale. A 50% cost saving is made after only a few units.]

Figure 5 shows a cross-section of the unit costs for each stage at quantities of 1 and 20. At production volumes of 1, the fully 3D printed step 0 has the lowest average cost due to its lack of set-up cost. At production volumes of 20, the the fully standardised design (step 7) achieves the lowest unit cost, demonstrating the economic advantages of conventional manufacturing methods at higher volumes.

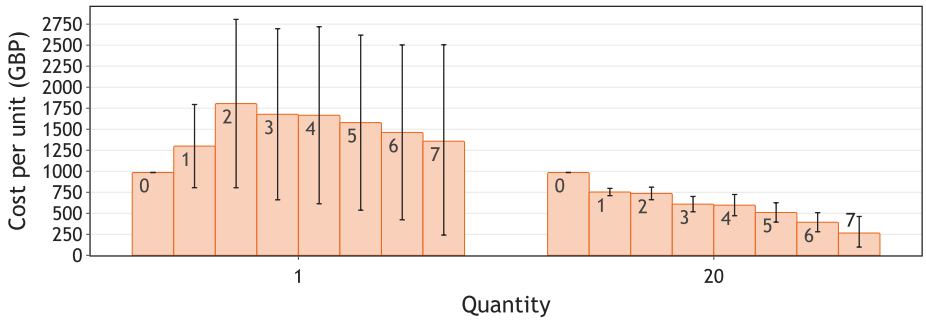

Figure 5. Cost per unit for the generated bracket (step 0) and steps 1 to 7 (left-to-right) for quantities of 1 unit and 20 units. Error bars show the minimum and maximum values based on the input ranges provided to the cost model

4.2. Performance

Three part metrics were used to assess performance: maximum deflection, part mass, and maximum von Mises stress. The metrics were assessed for the resulting part from each step. They are reported in figure 6, normalised by the values for the generative part to give relative performance to the original design.

The maximum deflection was not affected by the replacements made in steps 1 and 2, representing a volume replacement of 50%. Beyond that point, the deflection worsens for one step, and then improves. The deflection for step 7 (100% replacement) is 13% less (better) than the generatively designed part. The best performing part was step 6 (89% replacement) which deflected by 14.3% less than the generative part. The absolute values for the deflection are small (0.04 mm for the generative part) but are proportional to the force used in the FEA, so only the relative values are relevant.

The mass of the parts from steps 1 to 3 is the same as the generative part. Step 4 represents a 9% increase in mass relative to the generative part (worse). Step 6 has the highest relative mass, an 11% increase. The fully-replaced part shows a 9% increase, resulting in a stiffer but heavier design.

The maximum stress is the metric most negatively affected by replacements. Step 5 represents a 40% increase (worse). The fully-replaced part has maximum stresses 58% higher than the generative part.

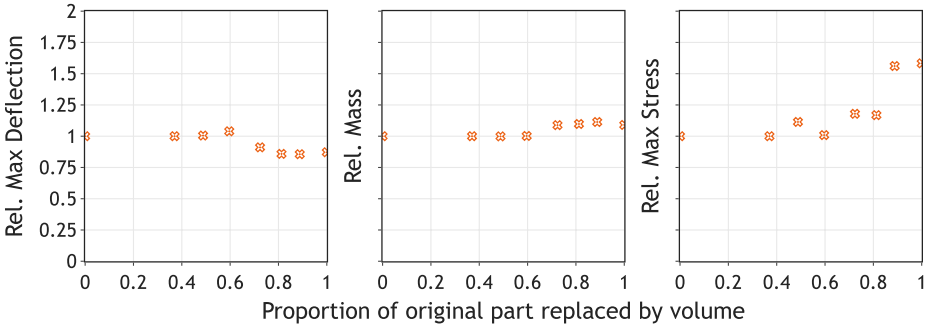

Figure 6. Performance of parts with varying amounts of their volume replaced with standard relative to the generative part. Left: maximum deflection, middle: mass, right: max stress (lower is better)

5. Discussion

For one-off production, there is a peak in cost for the intermediate stages, as shown in figure 5. These designs still have a substantial volume of 3D printed components (the main cost driver of the process), as well as the setup costs for machining and wire bending. At production quantities of 20, figure 5 shows an

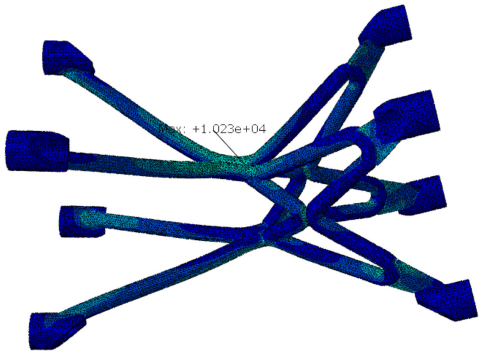

Figure 7. The von Mises stress on the underside of the bracket from step 7. The braze joint between wire forms introduces a stress concentration leading to the increase in peak stresses relative to the generative part

approximately linear decrease in unit cost through steps 0 to 7. At this quantity, setup costs have a small effect, and the volume of 3D printed parts remains the main driver of cost. This finding is consistent with the accepted wisdom that standardisation allows for economies of scale (Ulrich and Eppinger, 2000). The parity on all performance metrics for steps 1 to 3 reflects how closely the replacement parts approximate the geometry of the generated bracket. From step 4, the thinner struts on the loaded side of the bracket (right in figure 3) are replaced by the same 8 mm stock wire used throughout the design. The widening of the struts results in a heavier but stiffer part. The deviation from the generative design highlights the freedom available when approximating a generative part. In this case, the entire part is approximated with one diameter of wire, necessitating an some variation. Alternatively, multiple diameters of wire could be used, resulting in a better approximation, but necessitating a higher part count, management of multiple bar stocks, and more brazing joints.

This trade-off demonstrates the competing objectives in the replacement process. While this case study primarily focused on closely approximating the original part's geometry, an alternative approach could have prioritised matching or improving performance. For example, rather than using a wire, a wider tube with an equivalent mass per unit length (i.e., the same cross-sectional area) could have been employed. Although such a tube would maintain the same mass per unit length, its greater second moment of area would result in a geometrically different part with potentially lower deflection. The large step up in peak stress shown in the right-hand panel of figure 6 is located at the braze between bends highlighted in figure 7. The trade off between performance and manufacturability is explored in only some of the articles referenced in section 2. Weiss et al. (2018) reported a 2% penalty to their objective function when enforcing constraints. Shah et al. (2020) showed that penalty can vary significantly depending on the nature of the constraint as well as the design task. Enforcing a symetry constraint had a negligible effect for their "box" and "pedestal" tasks whereas extrusion constraint resulted in a 40% to 94% penalty. Given the discrete nature of a substitution method using standard components, a brazed joint is either present or absent, it is anticiapted that objectives such as mass and peak stress will vary stochastically.

This case study manually approximated sections of a GD part with beams. This approach was feasible because the GD process created beam-like structures. However, this method is not generally applicable. One of the substitution methods detailed in section 2 reported difficulties with parts having a volume fraction (material volume as a fraction of design space volume) greater than 0.2 (Watson et al., 2023). Beyond this threshold, fewer beam-like structures emerged, which inhibited their skeletonisation process. For other common TO objectives, such as heat transfer for designing 3D printed rocket nozzles or heat exchangers, intricate lattice structures are common features of generated parts. A substitution approach may be infeasible. In such instances, the second category approach of working with components directly may be preferable.

Acknowledgements

Jonathan Raines acknowledges financial support from the UKRI for a Centre for Doctoral Training studentship in Interactive Artificial Intelligence at the University of Bristol. (EP/S022937/1)

References

3MF Consortium (2021). 3MF. https://3mf.io/.

Aluminium Online (2024). Aluminium Round Bar 17.47mm (11/16”). https://www.aluminium-online.co.uk/product/11-16-aluminium-round-bar/. Online; accessed 2024-10-12.

Autodesk (2024). Autodesk Fusion. https://www.autodesk.com/uk/products/fusion-360/.

Barroqueiro, B., Andrade-Campos, A., and Valente, R. a. F. (2019). Designing Self Supported SLM Structures via Topology Optimization. *Journal of Manufacturing and Materials Processing*, 3 (3): 68.

Bends0e, M. P. and Kikuchi, N. (1988). Generating optimal topologies in structural design using a homogenization method. *Computer Methods in Applied Mechanics and Engineering*, 71 (2): 197–224.

Dassault Systèmes (2024). Abaqus CAE. https://www.3ds.com/products/simulia/abaqus/cae.

Fernández, E., Yang, K.-k., Koppen, S., Alarcón, P., Bauduin, S., and Duysinx, P. (2020). Imposing minimum and maximum member size, minimum cavity size, and minimum separation distance between solid members in topology optimization. *Computer Methods in Applied Mechanics and Engineering*, 368: 113157.

Greminger, M. (2020). Generative Adversarial Networks With Synthetic Training Data for Enforcing Manufacturing Constraints on Topology Optimization. In *ASME 2020 International Design Engineering Technical Conferences and Computers and Information in Engineering Conference*. American Society of Mechanical Engineers Digital Collection.

Guo, X., Zhang, W., and Zhong, W. (2014). Doing Topology Optimization Explicitly and Geometrically—A New Moving Morphable Components Based Framework. *Journal of Applied Mechanics*, 81 (081009).

Hicks, B. J. and Culley, S. J. (2002). Compatibility issues for mechanical system modelling with standard components. *Proceedings of the Institution of Mechanical Engineers, PartB: Journal of Engineering Manufacture*, 216 (2): 235–249.

Hicks, B. J., Culley, S. J., and Mullineux, G. (2002). Cost estimation for standard components and systems in the early phases of the design process. *Journal of Engineering Design*, 13 (4): 271–292.

Hoang, V.-N., Nguyen, N.-L., Tran, D. Q., Vu, Q.-V., and Nguyen-Xuan, H. (2022). Data-driven geometry-based topology optimization. *Structural and Multidisciplinary Optimization*, 65 (2): 69.

Huang, M., Cui, T., Liu, C., Du, Z., Zhang, J., He, C., and Guo, X. (2023). A Problem-Independent Machine Learning (PIML) enhanced substructure-based approach for large-scale structural analysis and topology optimization of linear elastic structures. *Extreme Mechanics Letters*, 63:102041.

Hypertherm Inc., USA (2024). Waterjet Cut Calculator. https://waterjet-calculator.hypertherm.com/. Online; accessed on 2024-12-03.

Lee, H. Y., Zhu, M., and Guest, J. K. (2022). Topology optimization considering multi-axis machining constraints using projection methods. *Computer Methods in Applied Mechanics and Engineering*, 390: 114464.

Li, Z., Xu, H., and Zhang, S. (2024). A Comprehensive Review of Explicit Topology Optimization Based on Moving Morphable Components (MMC) Method. *Archives of Computational Methods in Engineering*.

Materialise (2024). OnSite. https://onsite.materialise.com/en. Online; accessed 2024-11-11.

Metals Warehouse (2024). 2mm Aluminium Sheet. https://www.metalswarehouse.co.uk/product/2-0mm-aluminium-sheet/. Online; accessed 2024-10-12.

Nie, Z., Lin, T., Jiang, H., and Kara, L. B. (2020). TopologyGAN: Topology Optimization Using Generative Adversarial Networks Based on Physical Fields Over the Initial Domain. Volume 11A: *46th Design Automation Conference (DAC)*, page V11AT11A008.

Pahl, G. and Beitz, W. (1984). *Engineering Design A Systematic Approach*. Springer-Verlag, Berlin, 3rd edition.

PTC Inc (2024). Onshape. https://www.onshape.com.

Rochefort-Beaudoin, T., Vadean, A., Achiche, S., and Aage, N. (2024). From Density to Geometry: YOLOv8 Instance Segmentation for Reverse Engineering of Optimized Structures.

Sasaki, H. and Igarashi, H. (2019). Topology Optimization Accelerated by Deep Learning. *IEEE Transactions on Magnetics*, 55 (6): 1–5.

Seo, J. and Kapania, R. K. (2022). Development of Deep Convolutional Neural Network for Structural Topology Optimization. In *AIAA SCITECH 2022 Forum*, San Diego, CA & Virtual. American Institute of Aeronautics and Astronautics.

Shah, V., Kashanian, K., Pamwar, M., Sangha, B., Kim, I. Y., Shah, V., Kashanian, K., Pamwar, M., Sangha, B., and Kim, I. Y. (2020). Multi-Material Topology Optimization Considering Manufacturing Constraints. *SAE International Journal of Advances and Current Practices in Mobility*, 2 (6): 3268–3277.

Ulrich, K. T. and Eppinger, S. D. (2000). *Product Design and Development*. Irwin/McGraw-Hill, Boston, 2nd ed edition.

Watson, M., Leary, M., Downing, D., and Brandt, M. (2023). Generative design of space frames for additive manufacturing technology. *The International journal of Advanced Manufacturing Technology*, 127 (9): 4619–4639.

Weiss, B. M., Hamel, J. M., Ganter, M. A., and Storti, D. W. (2018). Data-Driven Additive Manufacturing Constraints for Topology Optimization. In *ASME 2018 International Design Engineering Technical*

Conferences and Computers and Information in Engineering Conference. American Society of Mechanical Engineers Digital Collection.
Yoon, G. H. and Ha, S. I. (2020). A New Development of a Shadow Density Filter for Manufacturing Constraint and Its Applications to Multiphysics Topology Optimization. *journal of Mechanical Design*, 143 (061703).
Yu, Y., Hur, T., Jung, J., and Jang, I. G. (2019). Deep learning for determining a near-optimal topological design without any iteration. *Structural and Multidisciplinary Optimization*, 59 (3): 787–799.
Zhang, W., Yuan, J., Zhang, J., and Guo, X. (2016). A new topology optimization approach based on Moving Morphable Components (MMC) and the ersatz material model. *Structural and Multidisciplinary Optimization*, 53 (6): 1243–1260.